Chemical Engineering Journal 315 (2017) 621–629

Contents lists available at ScienceDirect

Chemical Engineering Journal

journal homepage: www.elsevier.com/locate/cej

An easily prepared carbon quantum dots and employment for inverted organic photovoltaic devices

Xinyuan Zhang [a], Chunyu Liu [a], Zhiqi Li [a], Jiaxin Guo [a], Liang Shen [a], Wenbin Guo [a,*], Liu Zhang [b,*], Shengping Ruan [a], Yongbing Long [c]

[a] State Key Laboratory on Integrated Optoelectronics, College of Electronic Science and Engineering, Jilin University, 2699 Qianjin Street, Changchun 130012, China
[b] College of Instrumentation & Electrical Engineering, Jilin University, 938 Ximinzhu Street, Changchun 130061, China
[c] State Key Laboratory of Luminescence and Applications, Changchun Institute of Optics, Fine Mechanics and Physics, Chinese Academy of Sciences, 3888 Eastern South Lake Road, Changchun 130033, China

HIGHLIGHTS

- Dual electron transporting layer is used in organic solar cells.
- The energy barrier for electron transport is decreased.
- The balanced charge transfer of electron and hole is achieved.
- Well contact of active layer and cathode is realized.
- Electron extraction improvement by a good energy levels tailorment.

ARTICLE INFO

Article history:
Received 2 November 2016
Received in revised form 16 January 2017
Accepted 17 January 2017
Available online 19 January 2017

Keywords:
Electron transport and extraction
Self-assembled monolayer
Power conversion efficiency
Work function

ABSTRACT

In this paper, the performance enhancement of organic solar cells based on PCDTBT:$PC_{71}BM$ and P3HT:$PC_{60}BM$ are demonstrated via employing carbon quantum dots (CQD) to modify the metal oxide electron transport layer. The incorporated CQD with carboxylic acid (–COOH) groups could induce self-assembled monolayer (SAM) with TiO_2 buffer layer, which lowered the energy barrier for electron transfer and reduced the inherent incompatibility between the metal oxide and organic active layers. Further investigation shows that SAM of TiO_2 with CQD can improve the photo-induced exciton dissociation and charge transfer, leading to a low electron accumulation in charge transport layer and a reduced interface recombination loss.

© 2017 Elsevier B.V. All rights reserved.

1. Introduction

High efficiency organic bulk-heterojunction (BHJ) photovoltaics (OPVs) have been intensive studied because of low cost fabrication, facile processing methods, and portable energy source compared with Si-based inorganic solar cells [1,2]. Upon using new designed low bandgap polymers, controlling the active layer microstructure, and optimizing the device structure, the power conversion efficiency (PCE) of OPVs has been increased to more than 10% [3–7]. For practical applications, the inverted structure OPV (I-OPV), usually owns a metal oxide (such as TiO_x, ZnO) electron buffer layer (EBL) on ITO glass and high work function metal (Ag) as anode, which can improve air stability and manufacturing compatibility [8–14]. However, I-OPVs are still suffering from relatively lower PCE to meet the commercialization, possibly because the electrons are trapped on the interface between the active layer and the metallic oxide buffer layer, which are caused by the EBL surface defects as well as electron loss from slow charge injection due to the mismatch of work functions (WF) [15–18].

Several semiconductor materials have been used as the cathode interlayer for I-OPVs to lower the barrier of electron transfer from active layer to the ITO electrode. Among which titanium oxide (TiO_2) is one of the most extensively investigated to enhance the electron collection at the cathode for high efficiency and air-stable solar cells [19,20]. TiO_2 prepared by a simple sol–gel method is provided to be a multifunctional buffer layer including oxygen barrier, an optical spacer, and a hole blocking layer due to its merits of high electron affinity, high transparency, and excellent electrical/optical properties [21,22]. Nevertheless, the sol–gel EBLs still

* Corresponding authors.
E-mail address: guowb@jlu.edu.cn (W. Guo).

http://dx.doi.org/10.1016/j.cej.2017.01.067
1385-8947/© 2017 Elsevier B.V. All rights reserved.

suffer from some inadequacies, such as sensitive to moisture and the pin-holes introduced by thermal treatment lessen the blocking process, which are responsible for the loss of electron collection. The oxygen vacancies exist in TiO_2 film, which are energetically deep trap levels, inducing a severe recombination loss [23–26]. Moreover, a key limitation for high efficiency cells is that the electrical properties of the TiO_2 films are strongly related to the processing conditions. Therefore, the electron transport and collection may be less effective in TiO_2 buffer layer, and the highest reported electron mobility is $1.7 \times 10^{-4}\ cm^2\ V^{-1}\ s^{-1}$, which is still lower than that of polymer photo-layer and results in electron accumulation [27–30]. For these reasons, many efforts have been made to facilitate efficient electron transport, enhancing electroconductibility and suppressing trap-assisted recombination. For example, noble metal nanoparticles and quantum dots (QDs) materials have been used to dope into metal oxide and modify EBL surface with self-assembled monolayer (SAM) [31–36]. The SAM method provides a unique shortcut to regulate the physical and chemical properties of underlying substrate surfaces. On one hand, the SAM can adjust the surface energies and properties of underlying materials, which could promote the interfacial adhesion between the metal oxide EBL and the adjoining polymer photolayer [37–40]. On the other hand, the SAM can not only affect the electrical property but also tailor band alignment of the underlying film, and thus enhance charge transfer [41].

In this study, we prepared carbon quantum dots (CQD) by a facile way and capped it on the sol–gel TiO_2 as the combined electron transport layer (ETL) for I-OPVs. Compared with conventional semiconductor QDs, CQD with the virtues of similar fluorescence properties, excellent electrical conductivity, low cost, ease of synthesis, and low toxicity in addition to photochemical and chemical stability are employed to effectively modify EBL [42,43]. As the most popular materials, Poly [*N*-9″-hepta-decanyl-2,7-carbazo lealt-5,5-(4′,7′-di-2-thienyl-2′,1′,3′-benzothiadiazole)]:[6,6]-phe nyl C_{71}-butyric acid methyl ester (PCDTBT:PC_{71}BM) and poly(3-hex ylthiophene-2,5-diyl):[6,6]-phenyl-C_{60}-butyric acid methyl ester (P3HT:PC_{60}BM) are used as the BHJ active layer in I-OPVs system. Herein, we demonstrated a possible mechanism to explain the relation between EBL components, surface morphology, charge carrier transport properties, and electrical contact with photo-to-electrical energy conversion process. By applying a SAM TiO_2/CQD as EBL, the short-circuit current (J_{sc}) and fill factor (FF) are both increased and achieved a higher PCE, and thus proposes an attractive strategy for realizing roll-to-roll, high efficiency, and commercially available solar cell production.

2. Experimental

2.1. CQD Preparation and property

The microwave synthesis of CQD follows procedures given in our previous work [44,45]. A sample of the CQD was diluted in aqueous solution, which was purified in a centrifuge (10,000 r/min, 20 min) to remove large or agglomerated particles, and the sizes of left CQD are in the range from 1 to 5 nm. The schematic molecule structure of CQD is exhibited in Fig. 1a, and the substituent group of SAM that has great affinity to the surface –OH of TiO_2. CQD can be bound on the surface with –COOH group anchored surface with Ti–OH groups to form a carboxylate bond and the other one oriented towards vacuum.

2.2. Device fabrication and characterization

The devices were made with the structure of indium tin oxide (ITO)/titanium dioxide (TiO_2)/active layer/molybdenum oxide (MoO_3)/sliver (Ag), and the energy levels of all used materials are also shown in Fig. 1b. The patterned ITO-coated glass substrates were washed by acetone, anhydrous alcohol, and deionized water in sequence and subsequently dried with nitrogen. Anatase-TiO_2 layer (thickness of 40 nm) was prepared on the cleaned substrates using sol–gel method. For the control devices, the active layers (100 nm) of PCDTBT:PC_{71}BM and P3HT:PC_{60}BM were spin-coated on top of pristine TiO_2 films and annealed for 20 min in glove box and named Device I and Device II, respectively. While for the optimal devices, in order to form a SAM layer, the substrates with TiO_2 films were first immersed into the low concentration aqueous alkaline solution for 6 h. Then, the prepared CQD solutions with different concentrations of 1.2, 2.8, and 4.0 mg/mL were spin-coated on the top of hydroxylation processed TiO_2 with 5 min thermal treatment at 100 °C. The detailed process of SAM is demonstrated in Fig. 3. The active films were forming on different concentrations of CQD modified EBLs under the same condition with control devices. These cells with structure of ITO/TiO_2/CQD/active layer/MoO_3/ Ag are named as Device A, B, and C for PCDTBT system, and Device D, E, and F for P3HT system, respectively. Furthermore, in order to facilitate comparison, the devices with structure of ITO/TiO_2/CQD/active layer/MoO_3/Ag were made with CQD directly spin-coating on TiO_2 film without SAM process and the corresponding cells are named as Device a, b, c, d, e, and f accordingly. Finally, the OPVs were finished by thermal evaporation of 4 nm MoO_3 and 100 nm Ag as a hole transport layer (HTL) and electrode without encapsulation. All the other experimental parameters were based on previous experience. The active area of the device was about 0.064 cm^2.

Atomic Force Microscope (AFM) images in tapping mode were carried out using a Veeco multimode with a nanoscope III controller. Current density–voltage (J–V) characteristics of the finished devices were measured using a computer-programmed Keithley 2400 source/meter under AM 1.5G solar illuminations with an Oriel 300 W solar simulator intensity of $\sim$100 mW cm^{-2} (about one sun) in air. The light intensity was measured with a photometer (International light, IL1400) corrected by a standard silicon solar cell. The incident photon-to-current efficiency (IPCE) was measured with Crowntech QTest Station 1000 AD. The absorption and transmittance spectra were measured by means of ultraviolet/visible spectrometer (UV 1700, Shimadzu).

3. Results and discussion

As shown in Fig. 2, the SAM processes including three steps in our experiment (I) The hydroxylate of TiO_2, in which the -OH or O (oxygen atom) will facilitate adsorbed onto the film surface, and Ti (Titanium atom) will has a positive charge (M^+). (II) The neutralization reaction of strong Lewis acidic and alkali. Carboxyl groups with a negative charge caused by ionization will ionic bond with the M^+ firmly and the ionized H^+ will integrate the –OH or O resulted into –OH or H_2O. (III) Electrostatic interaction leads to an immediate and uniform formation of strong dipoles matrix pointing toward the surface of TiO_2 induced by electron-withdrawing terminal functional group of SAM [46–48]. Employing a thin SAM CQD interlayer can induce an interfacial dipole and thereby reduce the work function (WF) of ETL in theory. More importantly, Carboxylic-acid linkages tend to be more stable than $-NH_2$ (ammonium groups) and –OH bonds under wet conditions. Even under dry condition, the pressure of 10–12 atmosphere are required to reduce a full monolayer to half coverage, which was investigated by Moreira [49].

The interaction between the oxide and organic materials is immensely vital in dominating the surface property and interfacial

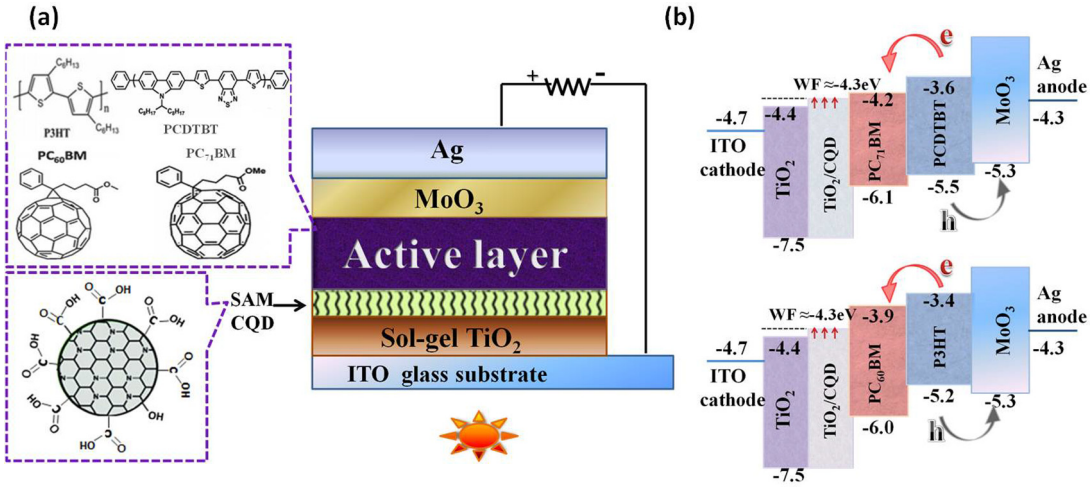

Fig. 1. (a) Schematic representation of I-OPVs structure and molecular structures of materials involved in this study. (b) Energy level diagram in I-OPVs based on PCDTBT: $PC_{71}BM$ and P3HT:$PC_{60}BM$ active layer.

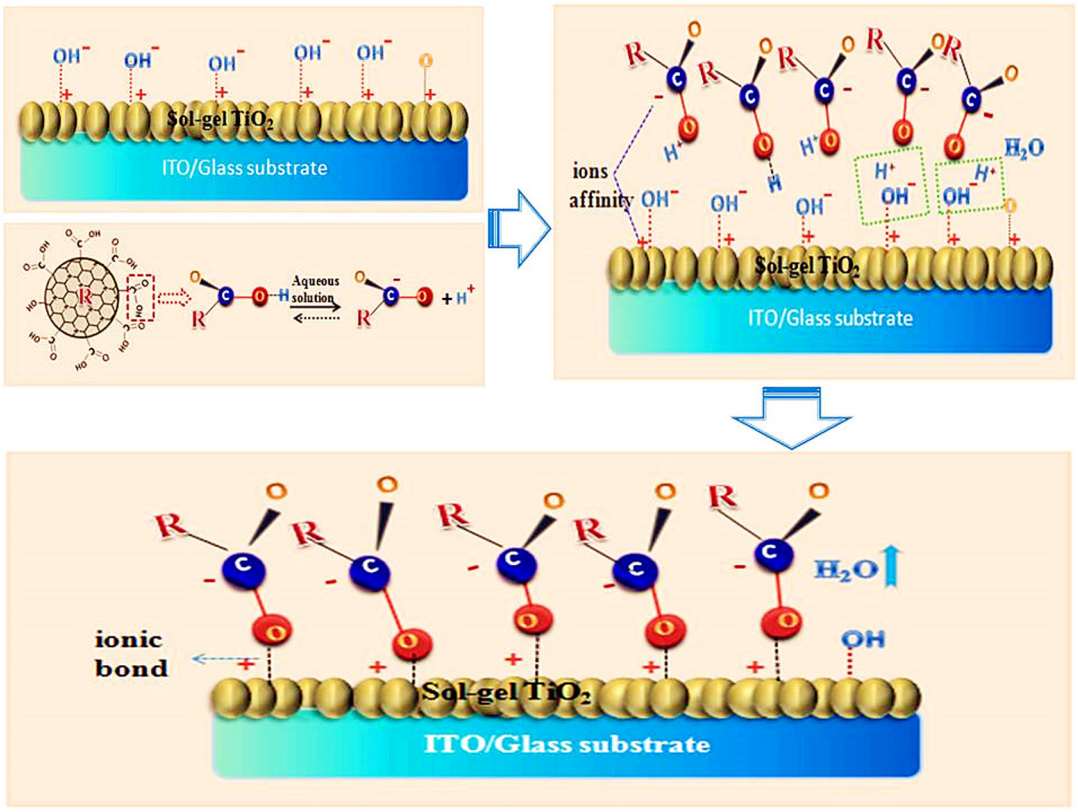

Fig. 2. (I) Hydroxylation process of TiO_2 film; Protonation of –COOH group suspended on CQD molecule, (II) Self-assemble of CQD deposition on TiO_2 film surface, (III) TiO_2/SAM CQD films.

energy-level alignment. At the initial of our study, Kelvin probe system was carried out to obtain the work functions (WF) of ETL surface. The recorded values of WF were 4.42 eV and 4.31 eV for TiO_2 and TiO_2/CQD respectively. For desired electron transport, the lowest unoccupied molecular orbital (LUMO) level of the acceptor material should be basically flat to the WF of the ETL. Therefore, the WF of TiO_2/CQD perfectly links up the LUMO of acceptor and TiO_2 ETLs, the electrons transport from active layer to the cathode is implemented with low energy barriers, resulting in a fast electron extraction.

As is well-known, surface wetting is an important factor for the solution coating process, and the water contact angles (WCA) of TiO_2 and TiO_2/CQD surface were measured. It can be seen in Fig. 3 that water droplets on TiO_2, TiO_2/CQD(non-SAM), and TiO_2/CQD(SAM) show the contact angles (θ) of 26.86°, 29.38°, and 42.16°, respectively. Both SAM TiO_2/CQD and non-SAM TiO_2/CQD surfaces exhibit an increased WCA than pristine TiO_2, indicating the well distributed CQD could be responsible for poor wetting. The incorporation of CQD by SAM process makes it more hydrophobic than pure TiO_2, which is beneficial for the

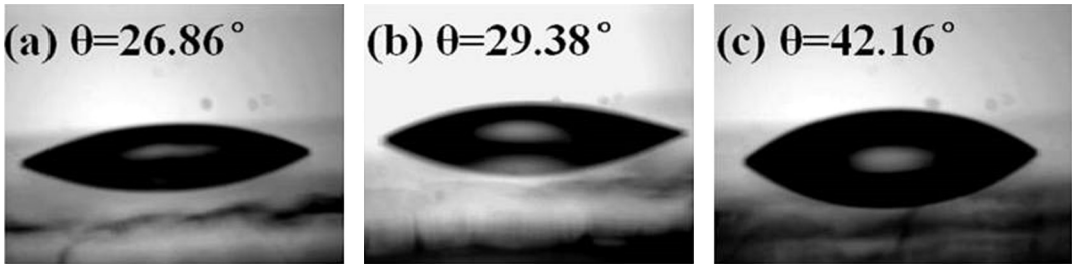

Fig. 3. Contact angles of the water-drops on the surface of (a) bare TiO_2, (b) TiO_2/non-SAM CQD, and (c) TiO_2/SAM CQD films.

spin-coating of active layer solution, leading to a better adhesion and filming property between metallic oxide ETL and organic photo-layer.

The illuminated J–V characteristics of the OPVs with or without CQD coated layer by SAM or non-SAM process are exhibited in Fig. 4. For the OPVs with PCDTBT:$PC_{71}BM$ active layer, the control device I without modification has a J_{sc} of 13.76 mA cm^{-2}, V_{oc} of 0.85 V, FF of 52.04%, yielding a PCE of 6.12%. For the devices with P3HT:$PC_{60}BM$ active layer, the control device II owns a J_{sc} of 13.01 mA cm^{-2}, V_{oc} of 0.58 V, FF of 49.11%, leading to a PCE of 3.73% in Fig. 4c. The performance of modified cells is improved at variety degrees mainly due to the enhancement of J_{sc} and FF while keeping V_{oc} in value. The cells with two different active layers own the highest efficiency with 2.8 mg/mL CQD solution modified TiO_2 no matter by SAM or non-SAM process, which are presented in Fig. 4b and d. Under the optimal concentration, the devices with a SAM modifier showed a better J_{sc} and FF compared to that with simply spin-coated CQD. The PCEs of Device B and E (SAM) are increased to 7.33% and 4.42%, accounting to a 19.77% and 18.50% enhancement. However, the PCEs of Device b and e (non-SAM) are increased to 6.87% and 4.10%, leading to 12.25% and 9.63% enhancement compared to control Device I and Device II. All the photovoltaic parameters of OPVs in this work are summarized in Tables 1 and 2 associated with PCDTBT and P3HT active layer, which are the average of 24 devices for every kind I-OPVs. Device A–F based on TiO_2/CQD(SAM) ETL show better performance improvement than Device a-f based on non-SAM CQD modified TiO_2 in particular on FF. Through calculating the slopes of the J–V curves, a relatively lower series resistance (R_s) with increased sharply shunt resistance (R_{sh}) was confirmed in the presence of the CQD. The R_s of OPVs stands for the resistance of the semiconductor bulk, the metal electrodes, and the metal/semiconductor interfaces. Correspondingly, R_{sh} basically illustrates the recombination of charge carriers at the interface and near electrodes [50]. The

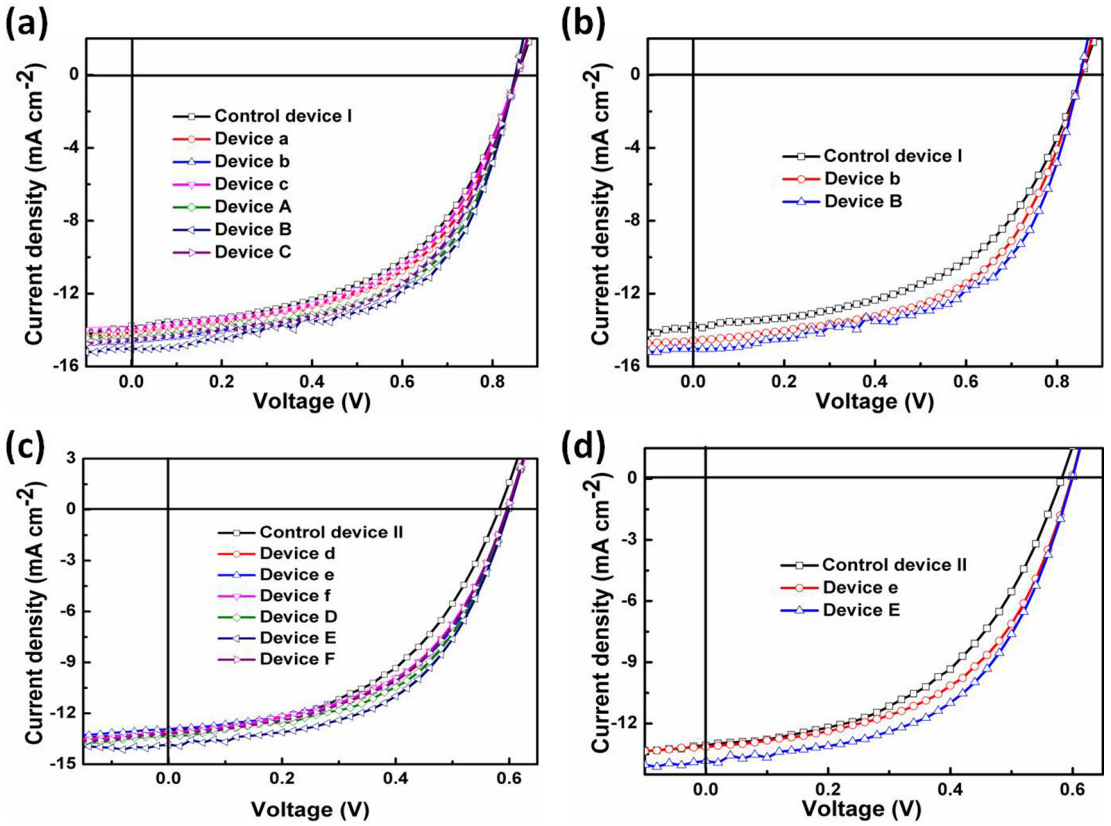

Fig. 4. The J–V characteristics of (a) control device, CQD modified cells with different concentration of 1.2 mg/mL, 2.8 mg/mL, and 4.0 mg/mL (Device a–c: non-SAM CQD, Device A–C: SAM CQD) based on PCDTBT active layer. (b) I-OPVs without and with optimized concentration of CQD modification by non-SAM and SAM process based on PCDTBT active layer. (c) Control device, CQD modified cells with different concentration of 1.2 mg/mL, 2.8 mg/mL, and 4.0 mg/mL (Device d–f: non-SAM CQD, Device D–F: SAM CQD) based on P3HT active layer. (d) I-OPVs without and with optimized concentration of CQD modification by non-SAM and SAM process based on P3HT active layer.

Table 1
Characteristics of PCDTBT:$PC_{71}BM$ I-OPVs based on TiO_2, TiO_2/non-SAM CQD (Device a–c) and TiO_2/SAM CQD (Device A–C) as electron transport layer (ETL) with different concentration of 1.2 mg/mL, 2.8 mg/mL, and 4.0 mg/mL CQD.

Device	V_{oc} (V)	J_{sc} (mA cm^{-2})	FF (%)	PCE (%)	R_s (Ω)	R_{sh} (Ω)
I	0.85 ± 0.02	13.76 ± 0.13	52.04 ± 0.01	6.12 ± 0.11	234.31	2522.4
a	0.85 ± 0.04	14.13 ± 0.11	53.58 ± 0.03	6.46 ± 0.11	189.80	6524.2
b	0.85 ± 0.02	14.58 ± 0.09	55.23 ± 0.03	6.87 ± 0.09	169.87	6229.7
c	0.85 ± 0.05	13.93 ± 0.12	52.95 ± 0.04	6.29 ± 0.13	191.97	8033.7
A	0.85 ± 0.02	14.48 ± 0.09	56.60 ± 0.02	6.97 ± 0.11	158.82	12365.0
B	0.85 ± 0.01	15.02 ± 0.08	57.36 ± 0.02	7.33 ± 0.12	145.32	21301.6
C	0.85 ± 0.03	14.51 ± 0.12	55.35 ± 0.01	6.86 ± 0.13	161.96	9277.3

Table 2
Characteristics of P3HT:$PC_{60}BM$ I-OPVs based on TiO_2, TiO_2/non-SAM CQD (Device d–f) and TiO_2/SAM CQD (Device D–F) as ETL with different concentration of 1.2 mg/mL, 2.8 mg/mL, and 4.0 mg/mL CQD.

Device	V_{oc} (V)	J_{sc} (mA cm^{-2})	FF (%)	PCE (%)	R_s (Ω)	R_{sh} (Ω)
II	0.58 ± 0.03	13.01 ± 0.13	49.11 ± 0.02	3.73 ± 0.12	165.71	4633.4
d	0.59 ± 0.02	13.13 ± 0.11	51.41 ± 0.03	4.05 ± 0.13	145.02	5994.2
e	0.59 ± 0.03	13.15 ± 0.11	52.17 ± 0.02	4.10 ± 0.10	142.94	7367.0
f	0.59 ± 0.04	13.17 ± 0.07	50.70 ± 0.05	3.99 ± 0.12	156.97	7288.9
D	0.59 ± 0.04	13.36 ± 0.09	52.94 ± 0.02	4.24 ± 0.09	140.17	17639.7
E	0.59 ± 0.02	13.84 ± 0.09	53.35 ± 0.03	4.42 ± 0.13	136.46	14569.0
F	0.59 ± 0.04	13.22 ± 0.10	51.38 ± 0.02	4.05 ± 0.11	141.81	6631.7

R_s was progressively decreased with CQD incorporation, especially for the case of SAM modified with 2.8 mg/mL CQD, which could be attributed to the enhanced charge carrier transport ability along TiO_2/CQD. This low electronic resistivity will facilitate charge carriers to transport from the bulk heterojunction composite to the respective electrodes. As a consequence, the inserted SAM CQD can effectively depress bulk recombination and reduce interfacial resistance, which accounts for FF increase of 8.22% and 8.63% for the best device with PCDTBT and P3HT system respectively. Due to the lower charge transfer and contact resistance, a larger electron extraction driving force can result in a larger J_{sc}. Furthermore, we have tried to modify TiO_2 buffer layer by just depositing thermally evaporated C_{60}. As results, the optimal devices show a little higher performance than control devices, but not as good as the devices modified with SAM process. Moreover, the evaporation process is more inconvenience and higher cost than the SAM process. The J-V characteristics and IPCE curves of control devices, devices with evaporated C_{60}, and SAM modified devices are shown in Fig. S1 (Supporting Information), and all the performance data are summarized in Table S1 (Supporting Information).

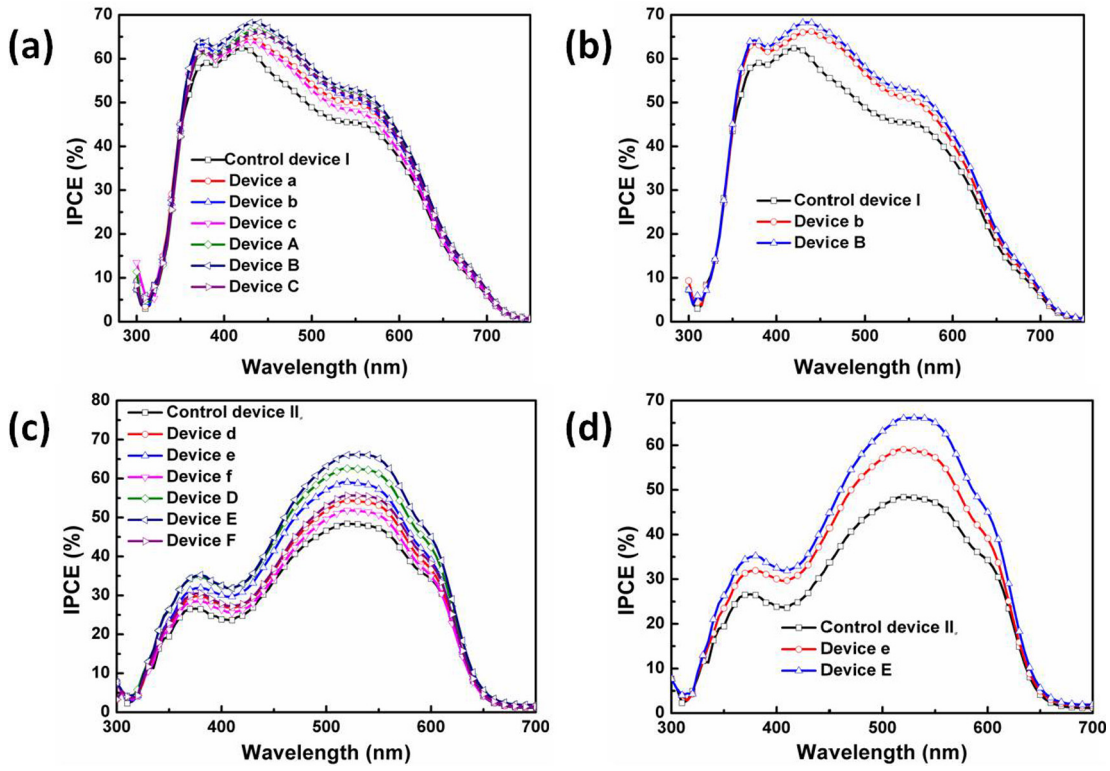

Fig. 5. IPCE spectrum of (a) control device, non-SAM CQD modified cells (devices a–c) and SAM CQD modified cells (device A–C) based on PCDTBT active layer. (b) Devices with TiO_2, TiO_2/non-SAM CQD, and TiO_2/SAM CQD as ETL with optimized concentration of CQD (2.8 mg/mL) for PCDTBT active layer. (c) Control device, non-SAM CQD modified cells (devices d–f) and SAM CQDs modified cells (device D–F) with CQD based on P3HT active layer. (d) Devices with TiO_2, TiO_2/non-SAM CQD, and TiO_2/ SAM CQD as ETL with optimized concentration of CQD (2.8 mg/mL) for P3HT active layer.

Therefore, it can be concluded that the SAM CQD modified OPVs present the best device performance because of the optimization of EBL surface energy and morphology, which resulted in the best contact with the active layer on top. The simple spin-coated process of modifier leads to the formation of particulate clusters rather than well arranged CQD, which may contribute to the insufficient interfacial adhesion with photo-layer as well as a discontinuous electron transport through the clusters, thus the performance of Device a-f (non-SAM) are inferior good. In addition, the concentration of CQD increased over 4.0 mg/mL, the PCEs of devices were slightly declined, which may be ascribed to the reduced light absorption of active layer and SAM interface properties.

To deeply understand the mechanism of J_{sc} improvement, the IPCE spectra of the devices were indicated in Fig. 5. Both IPCE of two kinds of modified devices are higher than that of control device over the almost entire wavelength range, especially from 350 nm to 625 nm, and the dependence of IPCE data on the concentrations of CQD are in good agreement with J–V characteristics. It is worth pointing out that the devices with TiO_2/CQD (SAM) ETL show the highest IPCE values, following by the devices with composite TiO_2/CQD(non-SAM) and the reference devices. For the devices with PCDTBT as electron donor (Fig. 5b), the IPCE of global optimum device B shows the maximum of ~68% around 440 nm, which is higher than that of the control device I (~60% at 420 nm). For the devices with P3HT:PC_{60}BM as active layer (Fig. 5d), the IPCE of the reference device II shows a maximum of ~46%, while the IPCE of the optimal device E with a SAM ETL is the maximum value of ~67% around 525 nm, which is also much higher than that of the control device. The largest improvement of IPCE values for two different active layer compounds were observed in the wavelength range where the reference device showed the highest IPCE, which indicates that the charge transport capacity enhancement of the devices with SAM CQD and non-SAM CQD effectively prevented carrier recombination,

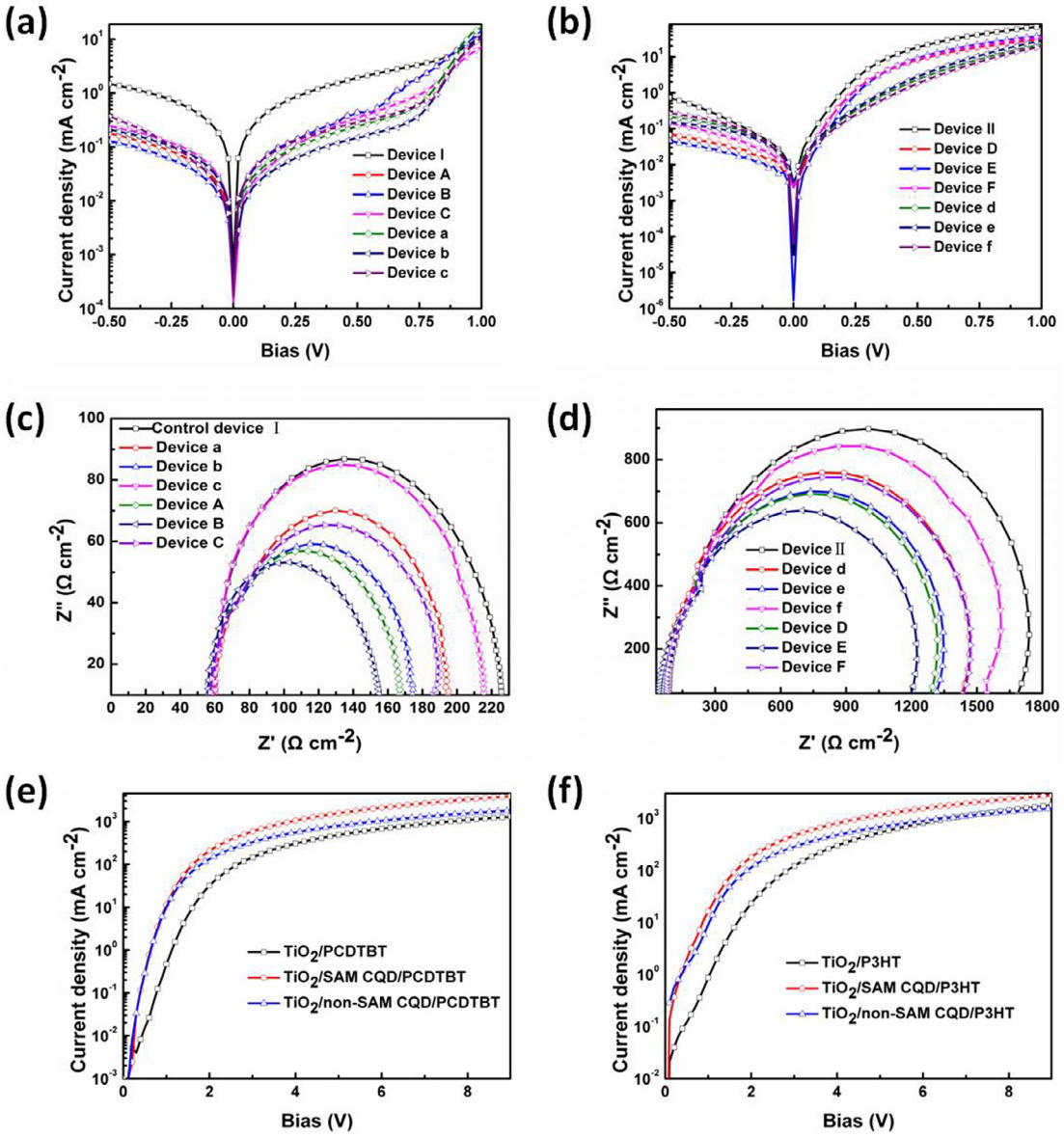

Fig. 6. The J–V characteristics of devices without and with different concentration of CQD modification by non-SAM and SAM process based on (a) PCDTBT:PC_{71}BM and (b) P3HT:PC_{60}BM active layer in dark. Nyquist plots of impedance spectra for OPVs based on (c) PCDTBT:PC_{71}BM and (d) P3HT:PC_{60}BM without and with different concentration of CQD by non-SAM and SAM method in dark. J–V characteristics of electron-only devices without and with 2.8 mg/mL CQD modification by non-SAM and SAM process for (e) PCDTBT:PC_{71}BM and (f) P3HT:PC_{60}BM active layer respectively. These data unraveled an excrescent shunt resistance (R_{sh}) and a smaller series or contact resistance (R_s) was obtained in SAM modified devices, implying that the EBL interface became more suited for electron transport and hole blocking, resulting in the increased FF and photocurrent. Moreover, the device under bias also showed larger injection current compared with the control device, which could prevent the current from leakage.

especially in the case of high photo-generated carriers [51–54]. Thereby, this observation provides a direct evidence for the increase of J_{sc}.

The dark J–V curves for all fabricated OPVs were presented in Fig. 6a and b. The devices A–F with TiO_2/CQD(SAM) exhibit excellent diode property and suppressed leakage current under reverse bias condition compared to the devices based on TiO_2/CQD(non-SAM) and pristine TiO_2.

To probe into the effect of SAM CQD on the electron transport and recombination, electrochemical impedance spectroscopy (EIS) of all the devices was tested under open circuit voltage condition from the frequency of 20 Hz to 20 MHz and shown in Fig. 6c and d. The semicircle's diameter in the Nyquist plots stands for the impedance values, which depends on charge transport at the interface between the photo-layer and electrode in the low-frequency region. Though Devices b and e with TiO_2/CQD(non-SAM) EBL exhibit slightly lower charge transfer resistance than the control Device I and Device II, the modification with a SAM CQD leads to a significant decline to impedance of device B and E, which presents a better interface was formed by introducing a SAM CQD coated layer. Thus, the injection barrier of electron was decreased, which effectively facilitated electron transfer from the active layer to cathode [55]. CQD with special structure could serve as a superfast bridge to facilitate the electron delivery, and thus refrained recombination loss from charge accumulation.

To verify the role of CQD on the electron mobility, the electron-only devices were fabricated with the structure of ITO/TiO_2/active layer/MoO_3/Ag, ITO/TiO_2/CQD(SAM)/active layer/MoO_3/Ag, and ITO/TiO_2/CQD(non-SAM)/active layer/MoO_3/Ag, respectively. The electron mobility was determined by fitting the dark current to the space charge limited current (SCLC) method [56]. As shown in Fig. 6e and f, the bare TiO_2 based device exhibited the relatively lower electron mobilities (μ_e) of 7.23×10^{-5} $cm^2 V^{-1} s^{-1}$ and 6.46×10^{-5} $cm^2 V^{-1} s^{-1}$ for PCDTBT and P3HT donors. After simply spin-coating CQD on TiO_2, the electron mobilities mildly increased to 6.22×10^{-4} $cm^2 V^{-1} s^{-1}$ and 5.33×10^{-4} $cm^2 V^{-1} s^{-1}$ respectively, which is credited to the fabulous nature electrical conductive property of CQD. Coupled with an excellent interlayer surface, the SAM CQD inserted devices displayed the highest electron mobilities of 8.43×10^{-4} $cm^2 V^{-1} s^{-1}$ and 8.22×10^{-4} $cm^2 V^{-1} s^{-1}$, which guaranteed a high mobility level of ETL at the same degree with active layer, and thus a more balance and unblocked charge carriers transport were achieved. As a consequence, an apparent increase of electron mobility leads to a more quickly migration of charge carrier and space charge formation decrease, resulting in the highest J_{sc} for SAM CQD based OPVs.

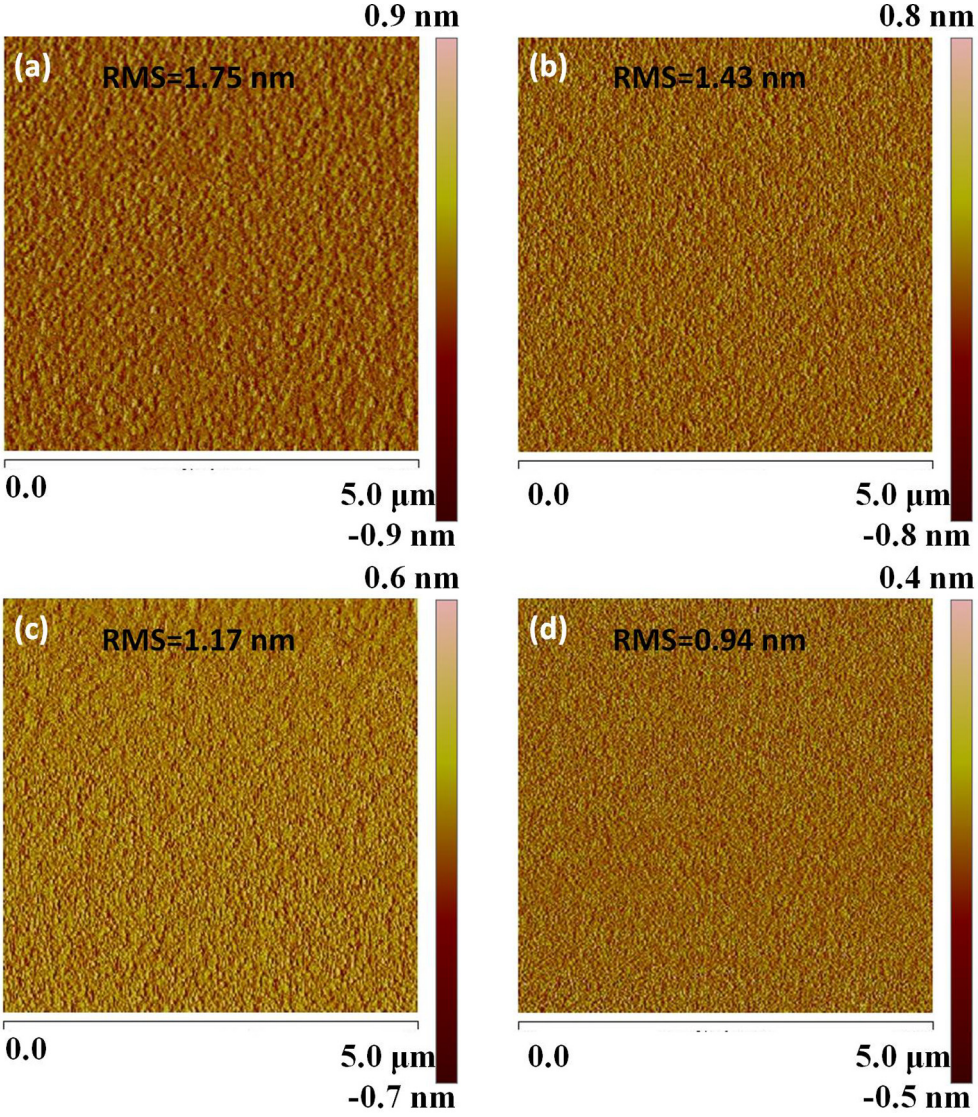

Fig. 7. AFM topography images of (a) TiO_2, (b) TiO_2/SAM CQD (1.2 mg/mL), (c) TiO_2/SAM CQD (2.8 mg/mL), and (d) TiO_2/SAM CQD (4.0 mg/mL) films.

In order to investigate the origin of the enhanced J_{sc} and FF, atomic force microscopy (AFM) was subsequently performed to explore the surface morphologies of the films without or with different kind modification process. Fig. 7a shows AFM images of the TiO_2 film and its surface root-mean square (RMS) roughness is 1.75 nm. After introducing SAM CQD on surface of sol–gel TiO_2 film with different concentration of 1.2, 2.8, and 4.0 mg/mL, the corresponding RMS roughness drops to 1.43 nm (Fig. 7b), 1.17 nm (Fig. 7c), and 0.94 nm (Fig. 7d). The film roughness is negative growth with CQD density. The smoother surface of TiO_2/CQD would be beneficial to form superior contact between the active layer and EBL, leading to a higher migration rate and a lower charge recombination. The slightly decrease of surface roughness might also increase the physical contact between EBL and the active layer. Additionally, we have checked the morphology of the active layers (PCDTBT:$PC_{71}BM$ and P3HT:$PC_{60}BM$) on differently modified TiO_2 buffers, and the results are shown in Figs. S2 (Supporting Information) and S3 (Supporting Information).The different modifications on TiO_2 had little influence on morphology of both two active layers. The active layers on TiO_2 active layers are slightly rougher than active layers on TiO_2 with SAM process, and smoother than the active layers on TiO_2 with CQDs by simply spin-coating.

Afterwards, the shunt resistance (R_{sh}) of the control and optimize devices were increased from 2522 Ω and 4633 Ω to 21,301 Ω and 14,569 Ω for PCDTBT and P3HT based devices (Tables 1 and 2), leading to a progressively increase of FF [57,58]. The presence of the SAM could flatten the peaks on the TiO_2 surface, which did not interfere the active layer coating and reduced the leakage current caused by these peaks [59,60]. Furthermore, the well-pressed underneath film likely causes smaller-scale phase separation of active layer and creates larger-area interfaces where charge separation can take place, contributing to an improved photocurrent and PCE. Though CQD modification with the biggest concentration results in the smoothest surface (Fig. 7d), the PCEs of the corresponding devices exhibit a slight decline for both active layers, which might be induced by the absorption decrease originating from the CQD addition. Generally, there are some protective groups in the surface of solution synthetic QDs materials, and the dielectric protective groups have a negative influence on charge transport, which must be removed before using in OPVs [61]. If there are no protective groups, the stability of the QDs will be decreased, and it is easy to aggregate [62]. As a result, the SAM TiO_2/CQD layer owns the better surface morphology than the simple spin-coated CQD on TiO_2. Above all, the smooth surface here suggests that the SAM process help to disperse CQD, suppressing the coverage photo-layer phase segregation beyond the molecular length scale. Not only because the SAM TiO_2/CQD induces fast electron transfer from polymer film, but also CQD reduces the defect sites density of metal oxide, which reveals potential and possibility for the ameliorate of electron transport property from a SAM TiO_2/CQD based device.

4. Conclusion

In conclusion, we have successfully developed I-OPVs using SAM TiO_2/CQD as a cathode interfacial layer, and the excellent electron transport capability of CQD was combined to TiO_2-based buffer layer device, which exhibited PCEs of 7.33% and 4.42%, significantly outperforming the reference devices by 19.77% and 18.50% for PCDTBT and P3HT system, respectively. The efficiency enhancement is mostly ascribed to the improvement of the photocurrent and substantial increase of FF. The WF of the SAM TiO_2/CQD layer was intermediate between the bare TiO_2 and LUMO of used acceptor materials, resulted in the decreased energy barrier for electron extraction. Moreover, AFM measurements have also verified that SAM CQD had a beneficial planarization effect, leading to a closer contact and therefore minimizing the contact resistance at the interface as indicated by the remarkable reduced R_s and improved R_{sh} values. Also, the improved morphology and electrical properties of TiO_2/CQD ETL reduced the interfacial charge recombination and improved FF in the SAM CQD containing devices. These findings about ETL modification by SAM technique provide an easy strategy to fabricate high performance I-OPVs.

Acknowledgments

The authors are grateful to National Natural Science Foundation of China (61275035, 61370046, 11574110), Project of Science and Technology Development Plan of Jilin Province (20130206075SF, 20140101060JC, 20150519003JH), the Opened Fund of the State Key Laboratory on Integrated Optoelectronics (IOSKL2013KF10) for the support to the work.

Appendix A. Supplementary data

Supplementary data associated with this article can be found, in the online version, at http://dx.doi.org/10.1016/j.cej.2017.01.067.

References

[1] C.J. Brabec, N.S. Sariciftci, J.C. Hummelen, Plastic solar cells, Adv. Funct. Mater. 11 (2001) 15–26.
[2] X.C. Li, F.X. Xie, S.Q. Zhang, J.H. Hou, W.C.H. Choy, Light: Sci. Appl. 4 (2015) e273.
[3] J. You, L. Dou, K. Yoshimura, T. Kato, K. Ohya, T. Moriarty, K. Emery, C.C. Chen, J. Gao, G. Li, Y. Yang, A polymer tandem solar cell with 10.6% power conversion efficiency, Nat. Commun. 4 (2013) 1446.
[4] Z.C. He, C.M. Zhong, S.J. Su, M. Xu, H.B. Wu, Y. Cao, Enhanced power-conversion efficiency in polymer solar cells using an inverted device structure, Nat. Photonics 6 (2012) 591–595.
[5] S.H. Liao, H.J. Jhuo, P.N. Yeh, Y.S. Cheng, Y.L. Li, Y.H. Lee, S. Sharma, S.A. Chen, Single junction inverted polymer solar cell reaching power conversion efficiency 10.31% by employing dual-doped zinc oxide nano-film as cathode interlayer, Sci. Rep. 4 (2014) 1.
[6] C.C. Chen, W.H. Chang, Y. Ken, O. Kenichiro, J.B. You, J. Gao, Z.R. Hong, Y. Yang, An efficient triple-junction polymer solar cell having a power conversion efficiency exceeding 11%, Adv. Mater. 26 (2014) 5670–5677.
[7] J.B. You, C.C. Chen, Z.R. Hong, K. Yoshimura, J.G. Li, Y. Yang, 10.2% power conversion efficiency polymer tandem solar cells consisting of two identical sub-cells, Adv. Mater. 25 (2013) 3973–3978.
[8] J.I. Nakamura, S. Suzuki, K. Takahashi, C. Yokoe, K. Murata, The photovoltaic mechanism of a polythiophene/perylene pigment two-layer solar cell, Bull. Chem. Soc. Jpn. 77 (2004) 2185–2188.
[9] K.S. Lee, J.A. Lee, B.A. Mazor, S.R. Forst, Transforming the cost of solar-to-electrical energy conversion: integrating thin-film GaAs solar cells with non-tracking mini-concentrators, Light: Sci. Appl. 4 (2015) e288.
[10] C. Edwards, A. Arbabi, G. Popescu, L.L. Goddard, Optically monitoring and controlling nanoscale topography during semiconductor etching, Light: Sci. Appl. 1 (2012) e30.
[11] Y.H. Su, Y.F. Ke, S.L. Cai, Q.Y. Yao, Surface plasmon resonance of layer-by-layer gold nanoparticles induced photoelectric current in environmentally-friendly plasmon-sensitized solar cell, Light: Sci. Appl. 1 (2012) e14.
[12] T.W. Lee, K.G. Lim, D.H. Kim, Approaches toward efficient and stable electron extraction contact in organic photovoltaic cells: inspiration from organic light-emitting diodes, Electron. Mater. Lett. 6 (2010) 41–50.
[13] S.K. Hau, H.L. Yip, O. Acton, N.S. Baek, H. Ma, A.K.Y. Jen, Interfacial modification to improve inverted polymer solar cells, J. Mater. Chem. 18 (2008) 5113–5119.
[14] M.S. White, D.C. Olson, S.E. Shaheen, N. Kopidakis, D.S. Ginley, Inverted bulk-heterojunction organic photovoltaic device using a solution-derived ZnO underlayer, Appl. Phys. Lett. 89 (2006) 143517-1–143517-3.
[15] Y. Zhou, H. Cheun, J.W.J. Potscavage, C. Fuentes-Hernandez, S.J. Kim, B. Kippelen, Inverted organic solar cells with ITO electrodes modified with an ultrathin Al_2O_3 buffer layer deposited by atomic layer deposition, J. Mater. Chem. 20 (2010) 6189–6194.
[16] S. Chen, J.R. Manders, S.W. Tsang, F. So, Metal oxides for interface engineering in polymer solar cells, J. Mater. Chem. 22 (2012) 24202–24212.
[17] K. Takahashi, I. Nakajima, K. Imoto, T. Yamaguchi, T. Komura, K. Murata, Sensitization effect by porphyrin in polythiophene/perylene dye two-layer solar cells, Sol. Energy Mater. Sol. Cells 76 (2003) 115–124.
[18] C. Waldauf, M. Morana, P. Denk, P. Schilinsky, K. Coakley, S.A. Choulis, C.J. Brabec, Highly efficient inverted organic photovoltaics using solution based titanium oxide as electron selective contact, Appl. Phys. Lett. 89 (2006) 233517.

[19] J.H. Park, T.W. Lee, B.D. Chin, D.H. Wang, O.O. Park, Roles of interlayers in efficient organic photovoltaic devices, Macromol. Rapid Commun. 31 (2010) 2095–2108.
[20] C.F. Guo, T.S. Sun, F. Cao, Q. Liu, Z.F. Ren, Metallic nanostructure for light trapping in energy-harvesting devices, Light: Sci. Appl. 3 (2014) e161.
[21] B.C. Park, S.H. Yun, C.Y. Cho, Y.C. Kim, J.C. Shin, H.G. Jeon, Y.H. Huh, I.C. Hwang, K.Y. Baik, Y.I. Lee, Surface plasmon excitation in semitransparent inverted polymer photovoltaic devices and their applications as label-free optical sensors, Light: Sci. Appl. 3 (2014) e222.
[22] A.K.K. Kyaw, X.W. Sun, C.Y. Jiang, G.Q. Lo, D.W. Zhao, D.L. Kwong, An inverted organic solar cell employing a sol-gel derived ZnO electron selective layer and thermal evaporated MoO_3 hole selective layer, Appl. Phys. Lett. 93 (2008) 221107.
[23] K. Takahashi, K. Seto, T. Yamaguchi, J.I. Nakamura, C. Yokoe, K. Murata, Performance enhancement by blending an electron acceptor in TiO2/polyphenylenevinylene/Au solid-state solar cells, Chem. Lett. 33 (2004) 1042–1043.
[24] K. Takahashi, Y. Takano, T. Yamaguchi, J.I. Nakamura, C. Yokoe, K. Murata, Porphyrin dye-sensitization of polythiophene in a conjugated polymer/TiO_2 p-n hetero-junction solar cell, Synth. Met. 155 (2005) 51–55.
[25] L.L. Huang, X.Z. Chen, B.F. Bai, Q.F. Tan, G.F. Jin, T. Zentgraf, S. Zhang, Helicity dependent directional surface Plasmon polariton excitation using a metasurface with interfacial phase discontinuity, Light: Sci. Appl. 2 (2013) e70.
[26] E.D. Kosten, J.H. Atwater, J. Parsons, A. Polman, H.A. Atwater, Highly efficient GaAs solar cells by limiting light emission angle, Light: Sci. Appl. 2 (2013) e45.
[27] C.H. Chou, W.L. Kwan, Z. Hong, L.M. Chen, Y. Yang, A metal-oxide interconnection layer for polymer tandem solar cells with an inverted architecture, Adv. Mater. 23 (2011) 1282–1286.
[28] T. Leijtens, G.E. Eperon, S. Pathak, A. Abate, M.M. Lee, H.J. Snaith, Overcoming ultraviolet light instability of sensitized TiO_2 with meso-superstructured organometal tri-halide perovskite solar cells, Nat. Commun. 4 (2013) 2885.
[29] S. Ito, S. Tanaka, K. Manabe, H. Nishino, Effects of surface blocking layer of Sb_2S_3 on nanocrystalline TiO_2 for $CH_3NH_3PbI_3$ perovskite solar cells, J. Phys. Chem. C 118 (2014) 16995–17000.
[30] X.J. Feng, K. Shankar, O.K. Varghese, M. Paulose, T.J. Latempa, C.A. Grimes, Vertically aligned single crystal TiO_2 nanowire arrays grown directly on transparent conducting oxide coated glass: synthesis details and applications, Nano Lett. 8 (2008) 3781–3786.
[31] Z. He, C. Zhong, S. Su, M. Xu, H. Wu, Y. Cao, Enhanced power-conversion efficiency in polymer solar cells using an inverted device structure, Nat. Photonics 6 (2012) 591–595.
[32] T. Yang, M. Wang, C. Duan, X. Hu, L. Huang, J. Peng, F. Huang, X. Gong, Inverted polymer solar cells with 8.4% efficiency by conjugated polyelectrolyte, Energy Environ. Sci. 5 (2012) 8208–8214.
[33] S. Khodabakhsh, B.M. Sanderson, J. Nelson, T.S. Jones, Using self-assembling dipole molecules to improve charge collection in molecular solar cells, Adv. Funct. Mater. 16 (2006) 95–100.
[34] S.H. Woo, W.H. Kim, H.J. Kim, Y.J. Yi, H.K. Lyu, Y.K. Kim, 8.9% single-stack inverted polymer solar cells with electron-rich polymer nanolayer-modified inorganic electron-collecting buffer layers, Adv. Energy Mater. 4 (2014) 1301962.
[35] D. Yang, L.Y. Zhou, W. Yu, J. Zhang, C. Li, Work-function-tunable chlorinated graphene oxide as an anode interface layer in high-efficiency polymer solar cells, Adv. Energy Mater. 4 (2014) 1400591.
[36] D. Yang, L.Y. Zhou, L.C. Chen, B. Zhao, J. Zhang, C. Li, Chemically modified graphene oxides as a hole transport layer in organic solar cells, Chem. Commun. 48 (2012) 8078–8080.
[37] C. Tao, S. Neutzner, L. Colella, S. Marras, A.R.S. Kandada, M. Gandini, M.D. Bastiani, G. Pace, L. Manna, M. Caironi, C. Bertarelli, A. Petrozza, 17.6% stabilized efficiency in low-temperature processed planar perovskite solar cells, Energy Environ. Sci. 8 (2015) 2365–2370.
[38] D. Yang, P. Fu, F.J. Zhang, N. Wang, J. Zhang, C. Li, High efficiency inverted polymer solar cells with room-temperature titanium oxide/polyethylenimine films as electron transport layers, J. Mater. Chem. A 2 (2014) 17281–17285.
[39] A. Loiudice, A. Rizzo, L.D. Marco, M.R. Belviso, G. Caputo, P.D. Cozzoli, G. Gigli, Organic photovoltaic devices with colloidal TiO_2 nanorods as key functional components, Phys. Chem. Chem. Phys. 14 (2012) 3987–3995.
[40] A. Tada, Y. Geng, M. Nakamura, Q. Wei, K. Hashimoto, K. Tajima, Interfacial modification of organic photovoltaic devices by molecular self-organization, Phys. Chem. Chem. Phys. 14 (2012) 3713–3724.
[41] H.S. Choi, J.S. Park, E.J. Jeong, G.H. Kim, B.R. Lee, S.O. Kim, M.H. Song, H.Y. Woo, J.Y. Kim, Combination of titanium oxide and a conjugated polyelectrolyte for high-performance inverted-type organic optoelectronic devices, Adv. Mater. 23 (2011) 2759–2763.
[42] S.S. Li, K.H. Tu, C.C. Lin, C.W. Chen, M. Chhowalla, Solution-processable graphene oxide as an efficient hole transport layer in polymer solar cells, ACS Nano 4 (2010) 3169–3174.
[43] J. Liu, Y. Xue, L. Dai, Sulfated graphene oxide as a hole-extraction layer in high-performance polymer solar cells, J. Phys. Chem. Lett. 3 (2012) 1928–1933.
[44] X.Y. Zhang, Z.Q. Li, Z.H. Zhang, C.Y. Liu, J.F. Li, S.N. Qu, W.B. Guo, Employing easily prepared carbon nanoparticles to improve performance of inverted organic solar cells, ACS Sustainable Chem. Eng. 4 (2016) 2359–2365.
[45] X.Y. Zhang, Z.Q. Li, Z.H. Zhang, C.Y. Liu, J.F. Li, W.B. Guo, L. Shen, S.N. Qu, Preparation and employment of carbon nanodots to improve electron extraction capacity of polyethylenimine interfacial layer for polymer solar cells, Org. Electron. 33 (2016) 62–70.
[46] Y.L. Wu, Y.N. Li, B.S. Ong, Printed silver ohmic contacts for high-mobility organic thin-film transistors, J. Am. Chem. Soc. 128 (2006) 4202–4203.
[47] Y.L. Wu, Y.N. Li, B.S. Ong, P. Liu, S. Gardner, B. Chiang, High-performance organic thin-film transistors with solution-printed gold contacts, Adv. Mater. 17 (2005) 184–187.
[48] C. Yee, G. Kataby, A. Ulman, T. Prozorov, H. White, A. King, M. Rafailovich, J. Sokolov, A. Gedanken, Self-assembled monolayers of alkanesulfonic and phosphonic acids on amorphous iron oxide nanoparticles, Langmuir 15 (1999) 7111–7115.
[49] N.H. Moreira, A. Domıinguez, T. Frauenheim, A.L. da Rosa, On the stabilization mechanisms of organic functional groups on ZnO surfaces, Phys. Chem. Chem. Phys. 14 (2012) 15445–154451.
[50] E.L. Ratcliff, A. Garcia, S.A. Paniagua, S.R. Cowan, A.J. Giordano, D.S. Ginley, S.R. Marder, J.J. Berry, D.C. Olson, Investigating the influence of interfacial contact properties on open circuit voltages in organic photovoltaic performance: work function versus selectivity, Adv. Energy Mater. 3 (2013) 647–656.
[51] H. Hoppe, N.S. Sariciftci, Organic solar cells: an overview, J. Mater. Res. 19 (2004) 1924–1945.
[52] C. Winder, N.S. Sariciftci, Low bandgap polymers for photon harvesting in bulk heterojunction solar cells, J. Mater. Chem. 14 (2004) 1077–1086.
[53] O. Blum, N.T. Shaked, Predication of photothermal phase signatures from arbitrary plasmonic nanoparticles and experimental verification, Light: Sci. Appl. 4 (2015) e322.
[54] D. Lepage, A. Jimenez, J. Beauvais, J.J. Dubowski, Real-time detection of influenza a virus using semiconductor nanophotonics, Light: Sci. Appl. 1 (2012) e28.
[55] H. Choi, H.B. Kim, S.J. Ko, J.Y. Kim, A.J. Heeger, An organic surface modifier to produce a high work function transparent electrode for high performance polymer solar cells, Adv. Mater. 27 (2015) 892–896.
[56] C. Goh, R.J. Kline, M.D. Mcgehee, E.N. Kadnikova, J.M.J. Frechet, Molecular-weight-dependent mobilities in regioregular poly(3-hexyl-thiophene) diodes, Appl. Phys. Lett. 86 (2005) 122110.
[57] X.X. Jiang, F. Chen, W.M. Qiu, Q.X. Yan, Y.X. Nan, H. Xu, L.G. Yang, H.Z. Chen, Effects of molecular interface modification in CdS/polymer hybrid bulk heterojunction solar cells, Sol. Energy Mater. Sol. Cells 94 (2010) 2223–2229.
[58] Y.Y. Liang, Z. Xu, J.B. Xia, S.T. Tsai, Y. Wu, G. Li, C. Ray, L.P. Yu, For the bright future-bulk heterojunction polymer solar cells with power conversion efficiency of 7.4%, Adv. Mater. 22 (2010) e135–e138.
[59] A. Ltaief, R.B. Chaabane, A. Bouazizi, J. Davenas, Photovoltaic properties of bulk heterojunction solar cells with improved spectral coverage, Mater. Sci. Eng. C 26 (2006) 344–347.
[60] D. Sahu, C.H. Tsai, H.Y. Wei, K.C. Ho, F.C. Chang, C.W. Chu, Synthesis and applications of novel low bandgap star-burst molecules containing a triphenylamine core and dialkylated diketopyrrolopyrrole arms for organic photovoltaics, J. Mater. Chem. 22 (2012) 7945–7953.
[61] T.D. Prichard, B.D. Vogt, Comparison of flocculated and dispersed single-wall carbon nanotube-based coatings using nonionic surfactants, Polym. Eng. Sci. 53 (2013) 69–77.
[62] H. Hong, X. Luan, M. Horton, C. Li, G. Peterson, Alignment of carbon nanotubes comprising magnetically sensitive metal oxides in heat transfer nanofluids, Thermochim. Acta 525 (2011) 87–92.